



Effect of indentation loading type on the mechanical properties of advanced high strength steel grade DP 800

Dursun Ekmekci¹ · Ömer Necati Cora²

Received: 12 February 2020 / Accepted: 20 October 2020 / Published online: 3 November 2020
© Springer-Verlag GmbH Germany, part of Springer Nature 2020

Abstract

The goal of this study was to acquire mechanical properties of a dual-phase grade advanced high strength steel (AHSS) by means of different microindentation loading conditions. Conventional, cyclic, and multi-step indentations were performed on DP 800 sample; and Young's modulus, hardness values were obtained by the depth-sensing indentation technique. Effects of different load levels (50–300 mN) and type of indentation on the results were also analyzed through ANOVA. The load levels experimented yielded overall material response rather than its constituents (e.g., martensite and ferrite). Both hardness and Young's modulus tend to decrease with increasing maximum indentation load level, especially from 50 to 100 mN, which is regarded as indentation size effect.

Keywords Microindentation · AHSS · Dual phase steel · Hardness · Young's modulus

1 Introduction

Automotive industry has been relentless in a quest for lighter and stronger vehicles for decades. Fuel efficiency, reducing tail-pipe emissions, improved safety are other hot topics for the automotive industry [1]. Advanced high strength steels (AHSS) along with lightweight Al and Mg alloys are among the primary choices to address these issues [2]. Nevertheless, their poor formability characteristics as well as relatively high cost over steel limits their adoption. Therefore, especially the auto industry, has been increasingly exploiting AHSS. Even though those have the same density with conventional steels, their utilization provide significant weight reduction as higher yield strength allows use of thinner gage thicknesses (e.g., in auto body closures). AHSS parts with 1100 MPa can provide 50–55% lightweighting [3]. Superior features of AHSS such as chemical composition and multiphase microstructure result of strictly controlled heating and cooling processes [4]. Advanced high strength steels can be categorized at least under six different groups including

micro alloyed steels, roll forming steels, martensitic steels, complex phase (CP) steels, bainitic steels, and dual phase (DP) steels. DP steels along with bainitic steels (e.g., TRIP steels) are the most commonly adopted AHSS types in auto industry. DP steels, consists of a soft ferritic matrix and hard martensite in the form of islands. This combination of hard and soft phase results in a superior strength-ductility balance. Therefore, they have been increasingly exploited in external body panels and structural members (e.g., bumpers, B-pillars, side impact beams, etc.). Transformation induced plasticity (TRIP) steels, on the other hand, exhibit better ductility at a given strength due to ferrite–bainite–austenite in their chemical composition. Improved formability is realized with the transformation of retained austenite to martensite during plastic deformation process [5]. Both DP and TRIP steels have increasingly been adopted in auto industry due to higher crash energy absorption so the increased passenger safety, increased crack resistance (e.g., high hole expansion ratio), and excellent ductility [6, 7]. The mechanical properties of the DP steels are primarily dependent on the volume fraction of its constituents, distribution and properties of the microstructural constituents [8].

Acquisition of mechanical properties of individual phases, on the other hand, can be realized by micro and nanoindentation technique [9–13]. Even though, the technique is relatively new, has progressed a lot since its first application in the 1980s, and the literature is abundant in terms of its application

✉ Ömer Necati Cora
oncora@ktu.edu.tr

¹ Department of Mechanical Engineering, Gümüşhane University, Gümüşhane, Turkey

² Department of Mechanical Engineering, Karadeniz Technical University, Trabzon, Turkey

to a variety of metallic materials [14–21]. In addition to metals, the technique can be utilized obtain the mechanical properties of thin films (e.g., PVD coatings), surface treatments, coatings (e.g., ceramics, nanocomposites etc.) [22–25]. Zhang et al. [26], in particular, sought to establish a relation between mechanical properties and microstructure of DP980. It was noted that the martensite hardness reduced significantly (from about 8.4 to 4.5 GPa) with increased annealing temperature. When the indents were made close to the interphase boundaries, the hardness was higher due to the high dislocation densities. Diego-Calderón et al. [27] carried out nanoindentation on quenched and partitioned (Q&P) steels. They reported nanohardness values of 7.6 GPa and 3.06 GPa, and Young's modulus values of 215.2 GPa and 197 GPa for untempered martensite and soft (ferrite) micro constituents, respectively, at 100 nm depth, and for indentation load of 1–2.5 mN. In another study by Ghassemi-Armaki et al. [28], the average nanoindentation hardness of ferrite was found to increase from 2 GPa in the as-received condition to 3.5 GPa in the specimen. Hardness of ferrite in the as-received condition was inhomogeneous: ferrite adjacent to ferrite/martensite interface was 20% harder than that in the interior. Hardness of the martensite, on the other hand, in as-received was reported to be in the range of 4.05–5.8 GPa for 80–130 nm indentation depth, and maximum indentation load of 2.5 mN. In another work [29], nanoindentation measurements were obtained on commercially-produced DP980 steels, yielding hardness value range of 3.5–4.5 GPa for ferrite, and 6.5–9.5 GPa for martensite at 40 nm indentation depth. Rodriguez et al. [30] studied the indentation size effect on different ferritic, pearlitic and martensitic steels by performing nanoindentation tests at different imposed depths (50–3000 nm). In general, the nanohardness was found to be slightly dependent on the imposed depth when the depth exceeds 1 μm . However, as the indentation depth decreases below 1 μm , a rapid increase of the nanohardness value was observed. For example, the hardness for the ferritic steel increases from about 1.85 to 3.3 GPa when the indent depth decreases from 1500 to 50 nm.

Current study, different from existing literature, aimed for obtaining mechanical properties of a dual phase steel grade, namely Docol 800 DP, with various types of indentation loading. Effect of different indentation testing procedures (conventional, cyclic, multi-step) on the results was studied. In addition, pile-up effect and hardness-strength relation of the material were also investigated.

2 Material and Methodology

2.1 Material

Material of interest was chosen as DP 800 (Docol 800 DP), and it was acquired from SSAB (Swedish Steel AB,

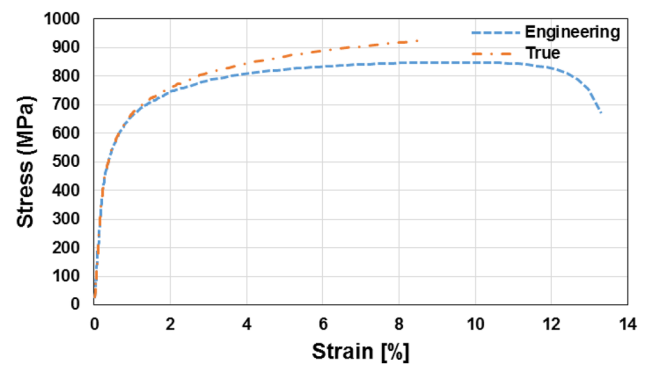


Fig. 1 Engineering and true stress–strain curves obtained from the uniaxial tensile test on DP 800

Table 1 Mechanical properties of Docol DP 800 [After 31]

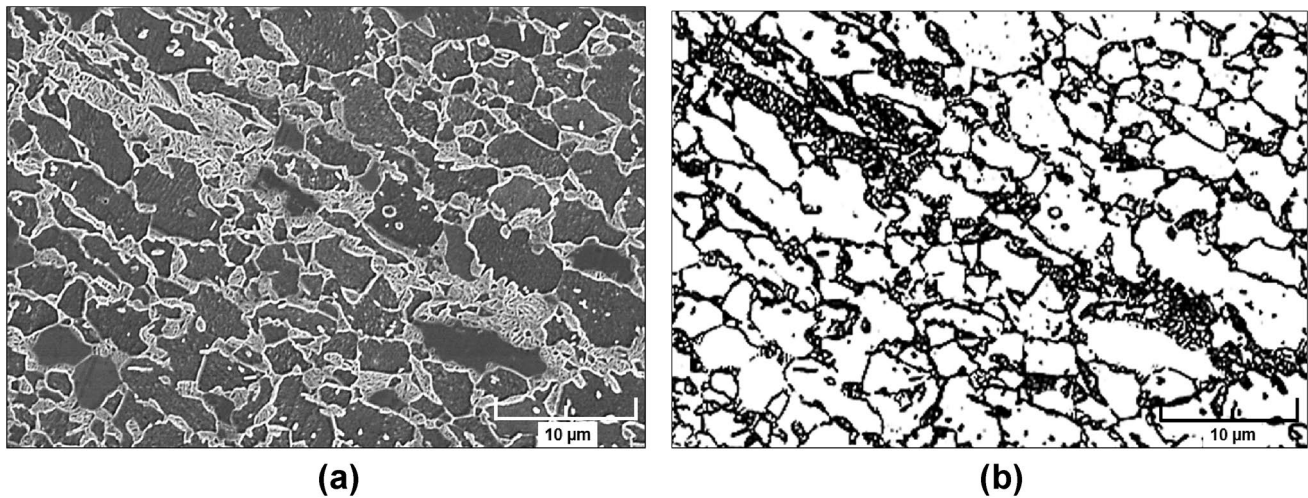
Yield strength (MPa) Min–Max	Tensile strength (MPa) Min–Max	Elongation (%) Min	HV _{0.2}
500–650	800–950	10	297

Borlänge, Sweden). It is a cold reduced dual phase steel subjected to special heat treatment in continuous annealing line, which produces a two-phase structure, namely ferrite and martensite. The ferrite provides unique forming properties, while hard martensite phase accounts for the strength. The strength of these steels increases with increasing martensite proportion in the microstructure [31]. Figure 1 shows the engineering and true stress–true strain curves obtained from the uniaxial tensile test for Docol DP 800. The mechanical properties and typical chemical composition of the material of interest are given in Tables 1 and 2, respectively.

Typical DP microstructure is in the form of soft ferrite matrix containing islands of harder martensite, as shown in Fig. 2. The soft ferrite phase is usually continual, giving these steels excellent ductility. When DP steels are deformed, strain is intensified in the lower strength ferrite phase surrounding the islands of martensite, and created high work-hardening ratio as ones of the characteristics of DP steels. The martensite volume was found to be around 33% in the microstructure. Wang et al. [32] determined the martensite volume of a DP800 material as 32%. As dual-phase steel microstructure contains distinct phases (e.g., soft ferrite, and hard martensite) significantly different mechanical properties have been reported in literature. The hardness of martensite can be as high as 10 GPa, while the hardness for ferrite is in the range of 3–7 GPa, in general. Contrary to hardness values, the grain sizes of both ferrite and martensite are in a narrow range of 1–10 μm , in most cases [26–29]. Nonetheless, indentation sizes greater than the individual grain size were recorded in the current study.

Table 2 Chemical composition of Docol DP 800 [31]

C%	Si%	Mn%	P%	S%	Al%	Nb%
0.15	0.20	1.50	0.01	0.002	0.040	0.015

**Fig. 2** **a** Microstructure of the DP 800; **b** binarization of the image for martensite volume fraction calculation

Therefore, the values obtained in current study stand for the overall material response rather than that for individual constituents.

2.2 Microindentation testing

Microindentation testing of dual-phase advanced high strength steel grade DP 800 was performed using UMT-2 Nano + Micro Tribometer (Bruker Inc.). Berkovich type indenter with $\nu_{\text{indenter}} = 0.07$ and $E_{\text{indenter}} = 1140$ GPa was employed to obtain the hardness and Young's modulus of the material in microindentation tests. While calculating Young's modulus, Poisson's ratio was assumed as 0.3 in Oliver–Pharr indentation method. All tests were performed at room temperature. Prior to measurements, the samples were mechanically polished with SiC sand papers with 320, 600, 1000, 1200, 1500 and 2000 grits, respectively. Then, fine polishing was performed on the sample surfaces with 1 μm diamond and 0.06 alumina suspensions. Three different test procedures (conventional, cyclic, multi-step) were applied for indentation. Indentations were performed at a contact force level from 0 to 300 mN with an increase of 50 mN at each indent. After each indentation, the tip was moved up (load removed completely), and a new indentation was performed at an increased load level. This type of indentation is referred as to “conventional” and the procedure was performed at least at 9 different locations to address the repeatability. In “multi-step” indentation, on the other hand, the indenter was not completely moved

up from the indent area after the preset value of maximum indentation force is reached. The sample reloaded to higher loads or depths upon previous loading cycle. On the other hand, “cyclic” indentation, facilitated the repeated indentation maximum force of 300 mN. During the indentations, the load rate was set to 0.1 mN/s and the indentation depth (nm) and the force (mN) were recorded with a PC. The raw data was then used to construct the P – δ plots, and hardness, and Young's modulus. In each type of measurement, the variation of material properties (e.g., Young's modulus and hardness) was analyzed to reveal the possible indentation size effect. It is reported in literature that material properties including Young's modulus and hardness can vary with the indentation load experimented [33, 34]. This phenomenon is named as indentation size effect. In addition, the statistical analyses were performed. One-way ANOVA tests (with $p < 0.05$) were executed to reveal the significance of variation on the data obtained. Figure 3 shows the 3×3 microindents obtained at 50 mN and 100 mN loads.

3 Results and discussion

3.1 Cyclic indentation

The cyclic loading in microindentation was performed at 300 mN indentation force with a repetition the cited load for 11 times at 9 different locations. Figure 4a shows the P – δ curves obtained for the DP 800. It can be seen that there is

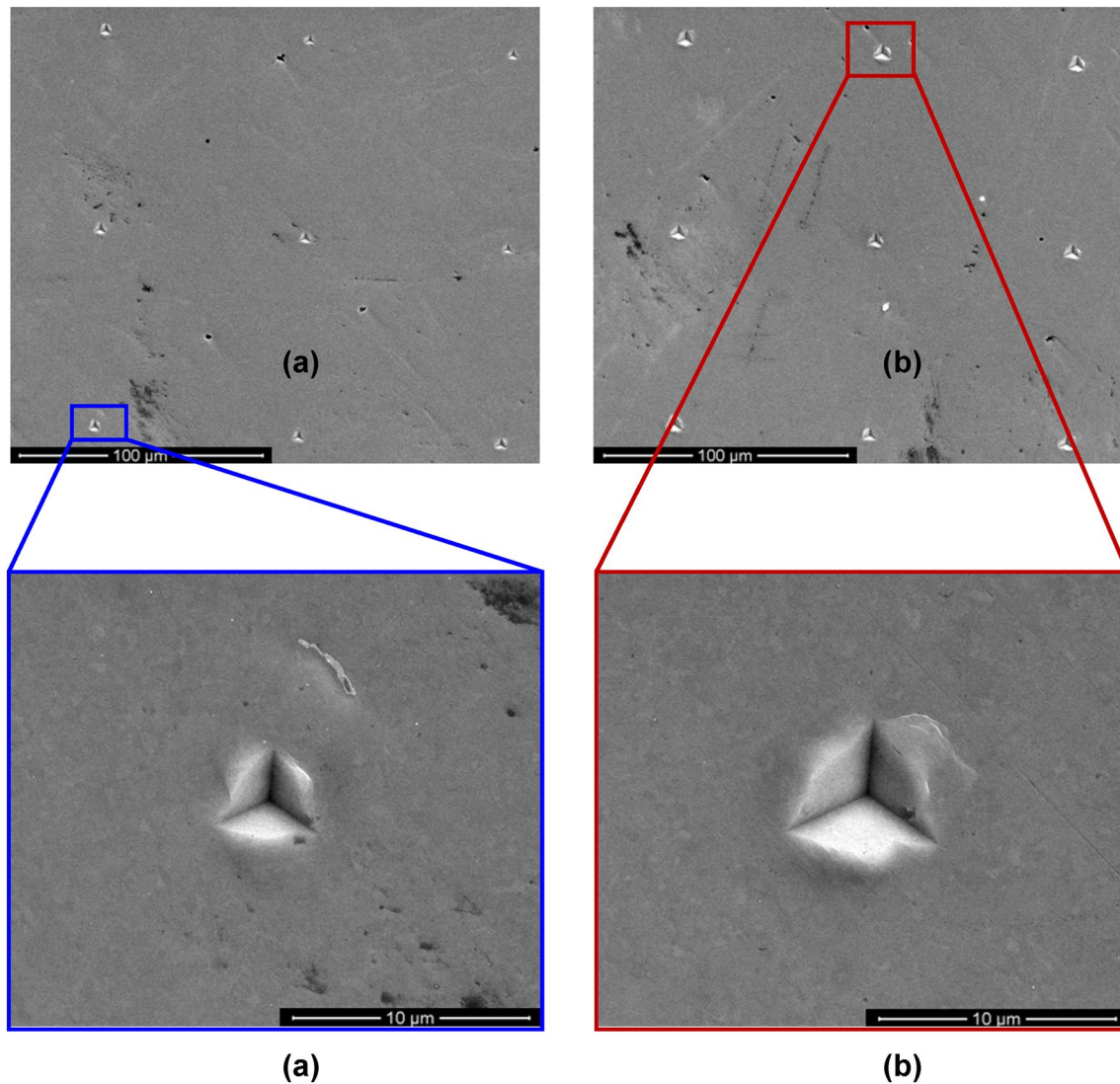


Fig. 3 **a** Nanoindentation applied at 50 mN load; **b** nanoindentation applied at 100 mN load

a trend for the indenter to penetrate shallower as cycling proceeds under a constant force. This can be attributed to the fact that the elastic recovery (so the final indentation depth) decreases with the repeated loading. Figure 4b shows the Young's modulus and hardness values obtained upon cyclic indentation with 300 mN constant peak force. The variations for both Young's modulus and hardness values can be explained by the spatial variation of the indentation on different locations, different constituents, grain size, defects, inclusions etc. [33]. Average hardness and Young's modulus values in cyclic indentation were obtained as 3.6, and 188 GPa, respectively. Cyclic loading is used to analyze microstructure-deformation mechanisms, dynamic deformation characteristics such as strain-hardening/softening, phase transformation under stress, fatigue, and fracture toughness of materials [29, 30]. For example, Saraswati et al. [36]

investigated dislocation–microstructure interactions in calcium-doped gold by means of cyclic nanoindentation. Chabok et al. [37] utilized cyclic nanoindentation to investigate the crack size and the conditional fracture toughness of weld zones on resistance spot welded DP 1000-GI dual phase high strength steel. In another work by Roa et al. [38], cyclic indentation experiments were performed to reveal the time-dependent response of an austenitic stainless steel.

3.2 Conventional indentation

Figure 5 shows the P – δ curves for DP 800 under conventional indentation at different load levels (e.g., 50, 100, 150, 200, 250, 300 mN). Measurements were conducted at 9 different locations. As it can be seen from Fig. 5a that characteristics of the loading and unloading curves

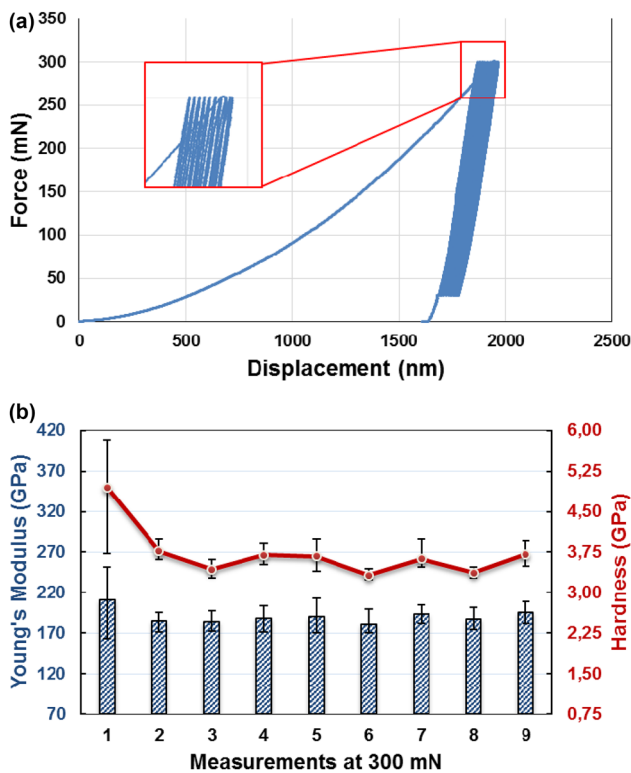


Fig. 4 **a** Example to indentation load vs. depth curves for cyclic indentation at 300 mN; **b** variation of Young's modulus (column), and hardness (line) at different measurements

for different peak loads are in quite well agreement with each other. Similar observations were reported for different materials by several researchers in literature [34, 55, 40]. A small pop-out towards the end of unloading curves implies that the phase transformation occurred from retained austenite to martensite, which results in volume increase in the vicinity of indent area and push back the indenter tip. Similar cases were reported for TRIP700 steel by Rijkenberg et al. [41], and for Si by Schuh [42].

Young's modulus and hardness values calculated from these indentations are also given in Fig. 5b, respectively. Young's modulus values were recorded in the range of 192–227 GPa, while hardness values were in the range of 3.17–3.62 GPa. A similar range of hardness values reported by Ruiz-Andres et al. [43] for DP 1000 steel when the indentation depth of 5 μm is employed. The trend for both Young's modulus and hardness data were observed to be similar, both decrease with increasing indentation force up to 250 mN even though the variations were not significant. The variation in hardness values was found to be in a narrow range. This implies that the indentation load levels are relatively high so that the obtained values refer to overall hardness rather than that for individual constituents as it was reported by Delincé et al. [44].

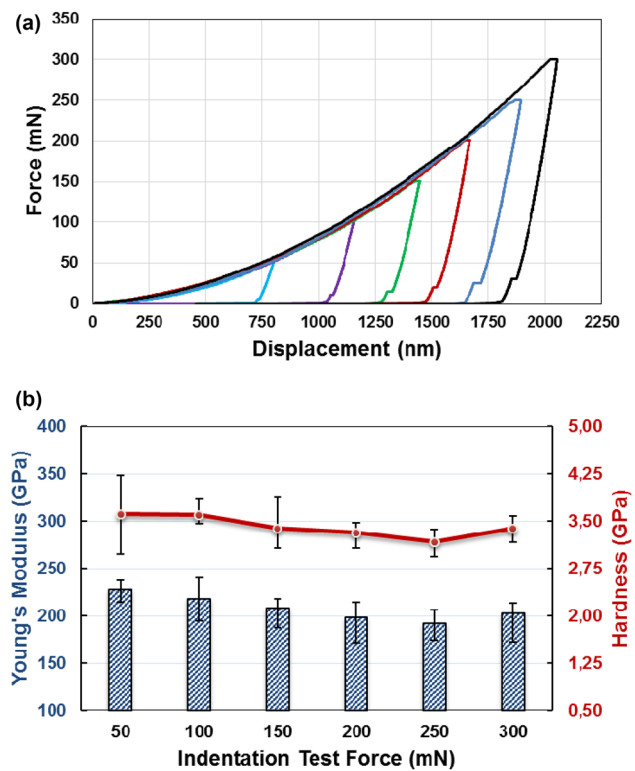


Fig. 5 **a** Typical indentation load vs. depth curve series for conventional indentation with different maximum indentation loads; **b** variation of Young's modulus (column), and hardness (line) with respect to indentation test force on DP 800

To reveal phases of microstructures, where indents were performed the microindented sample was etched for 5–10 s in Nital (5% HNO_3 and 95% Ethanol) solution. Figure 6 shows etched microindents which was obtained at 50 mN and 100 mN maximum loads. In agreement with literature, the martensite phase is observed in the form islands in ferrite matrix. It was clearly observed that all the indents were placed onto both martensite and ferrite phase rather than an individual one. Therefore, as discussed above, the measurements obtained are regarded as overall material response rather than one for a single phase.

3.3 Multi-step indentation

Multi-step indentation, on the other hand, is used to determine the mechanical properties at different depths using a single indent [34]. It is an useful tool to investigate the influence of microstructural evolution on successive deformation [45]. Strain rate sensitivity of a material can also be determined using multi-step nanoindentation [46]. In literature, multi-step indentation is used to study the phase transformation of materials [34, 35, 47]. With this type of loading, Young's modulus and hardness can be acquired as a function of indentation depth for both hard

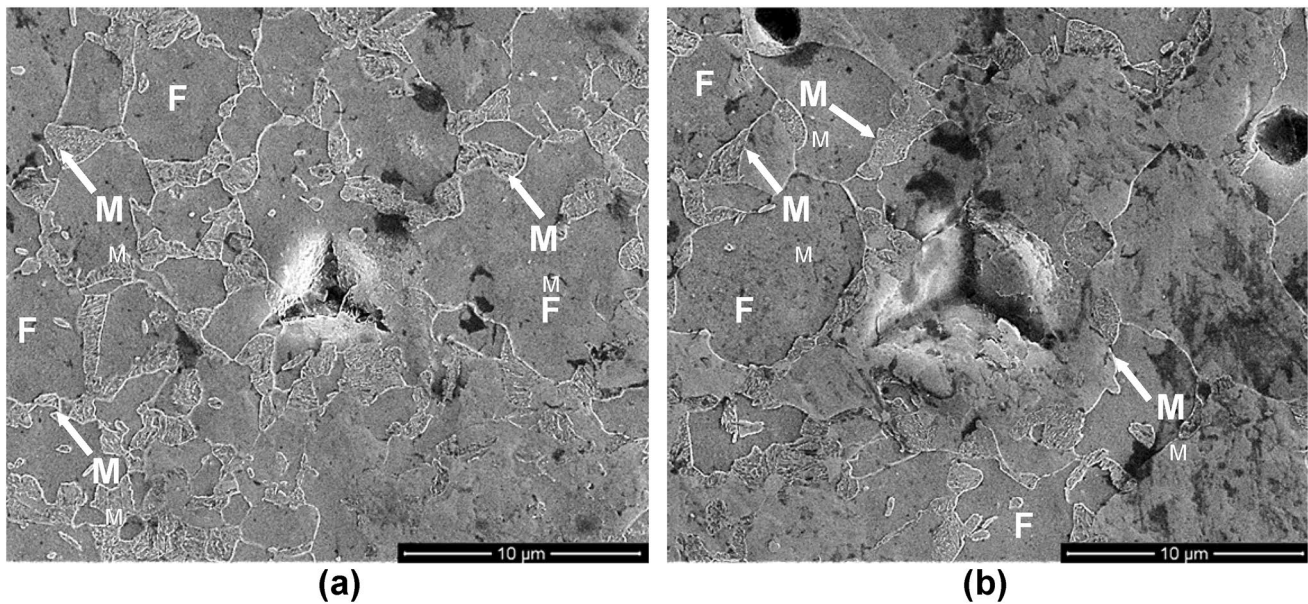


Fig. 6 **a** Etched surface image for conventional indentation at 50 mN; **b** Etched surface image for conventional indentation at 100mN (*F* Ferrite, *M* Martensite)

and soft materials [48, 49]. Multi-step indentations with increasing load levels from 0 to 300 mN were performed in this study. Figure 7a shows continuous measurement of indentation P – δ values. It was noticed the slope of the reloading curves are higher than that for loading curves. This can be attributed to the fact that the material gets work-hardened as the higher indentation forces are employed in each new loading. Figure 7b, on the other hand, shows Young's modulus and hardness variations at different indentation force levels. The trend observed for both Young's modulus and hardness values is similar, steady decrease in values with increasing indentation force. This can be explained with the fact that when the indentation depth increases the surrounding matrix (ferrite) acts as a soft substrate and the load is carried predominantly by the ferrite rather than martensite [44]. The hardness values decrease with increasing force up to 200 mN, and remains almost constant for the higher forces. The indentation size effect was found to be more pronounced in lower indentation forces or shallow indentation depths [50]. In agreement with the literature, the indentation size effect was noticeable in the range of 50–150 mN in the current study. Similar results were reported for different steels in literature [30, 51]. Additionally, the one-way ANOVA analysis was performed to examine the influence of different indentation forces on Young's modulus and hardness values by testing the hypothesis of the equality of arithmetic means.

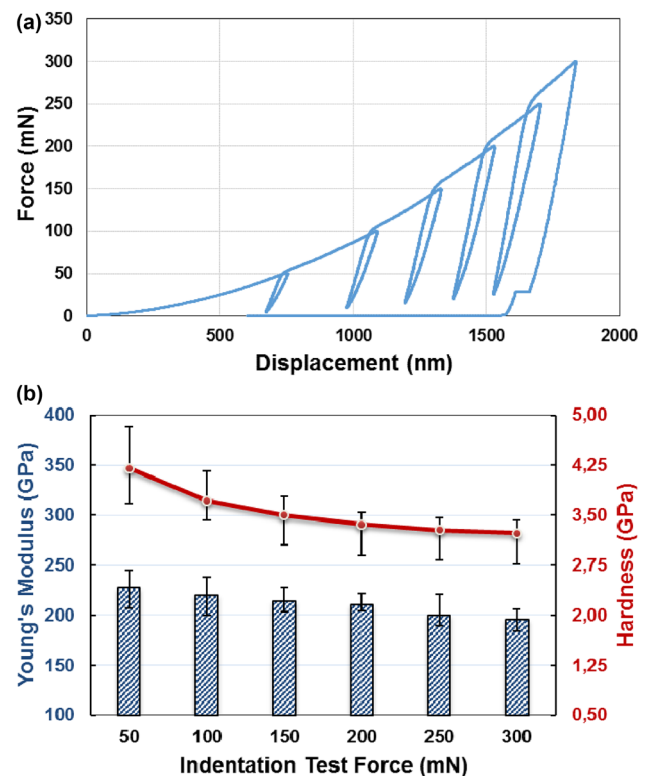


Fig. 7 **a** Representative indentation force–depth curve for multi-step indentation; **b** variation of Young's modulus (column), and hardness (line) with respect to applied test force on DP 800

3.4 Comparison of mechanical properties

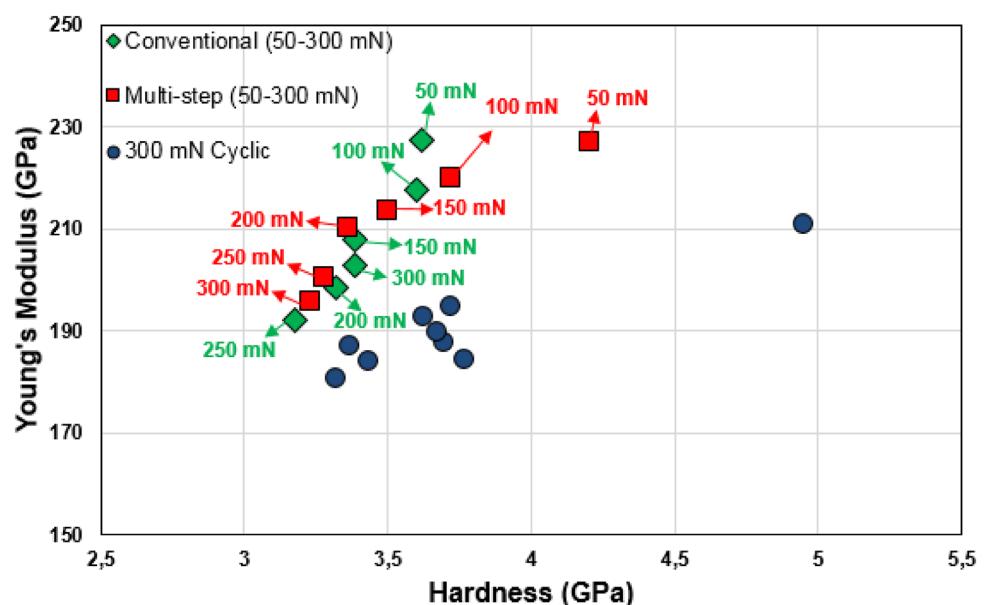
The relationship between the hardness and Young's modulus of DP 800 with three different tests is shown in Fig. 8. In all instances, the Young's modulus of the DP 800 material increases with increasing hardness. The Young's modulus data obtained through conventional and multi-step indentations were in quite well agreement. The same conclusion can be made for hardness values except the data obtained at 50 mN. When compared to literature, the hardness data was found to be in the reported hardness range of ferrite to martensite yet results obtained from indentations were in a narrow range. This was resulted from the load levels applied. Relatively lower indentation forces (e.g., up to 10 mN) were employed in the literature [52]. This lead to distinct hardness values referring to different phases (ferrite and martensite). The indentation forces experimented in the current study, on the other hand, yielded an overall hardness value of the material rather than its constituents [29]. Therefore, it is concluded that the values reported in the current study reflect the material's overall response. To investigate the mechanical properties of different phases, the indent area (so the indentation force level) should be selected smaller than the grain size of phases. In addition, the Young's modulus of the DP 800 in conventional indentation yielded the highest Young's modulus, while cyclic indentation at 300 mN constant load level the smallest value of same hardness values. Microindentation with the Berkovich pyramidal indenter and three various loading sequences were used to obtain elastic modulus and hardness of dual phase steel DP800. All results were statistically evaluated and compared. Although the alloy has two phases with different

mechanical properties, even the smallest maximum load level (50 mN) was sufficiently high to obtain general response of material.

3.5 Pile-up effect

During the indentation, plastically deformed material tends to flow-up against the faces of indenter and it is pushed away from the center of indent. This phenomenon is known as "pile-up" and it affects the calculated contact area, consequently the derived mechanical properties. h_f/h_{max} values (h_f is final indentation depth, and h_{max} is the maximum indentation depth) were calculated to reveal its possible existence. Theoretically, h_f/h_{max} ranges between 0 and 1. As the value approaches to zero, the material exhibit fully elastic behavior and hence all the deformations were removed during unloading stage. On the other hand, the material behaves in a rigid-plastic when the $h_f/h_{max} = 1$ in which elastic recovery (springback) does not occur. When $h_f/h_{max} \geq 0.7$, it is regarded as an indicator of a pile-up, while the ratio smaller than 0.7 is considered as a sign of sink-in. Upon calculations, h_f/h_{max} was found as greater than 0.7, in most cases in the current study. Nevertheless, there are variety of studies that reported different critical values for pile-up. Bolshakov et al. [53], for example, reported pile-up effect for aluminum when $h_f/h_{max} = 0.951$. Giannakopoulos et al. [14], on the other hand, suggested that the initial point for pile-up effect for h_f/h_{max} value of 0.875 for AISI 1070 ultra-high strength steel. In another study by Qian et al. [15], h_f/h_{max} was noted at higher than 0.8 for copper and stainless steel using the load range of 2–200 mN. Xu et al. [21] reported that not only the h_f/h_{max} ratio, but also the strain hardening exponent (n) of

Fig. 8 Relationship between hardness and Young's modulus for three different loading types adopted (conventional, multi-step and 300 mN cyclic) on DP 800



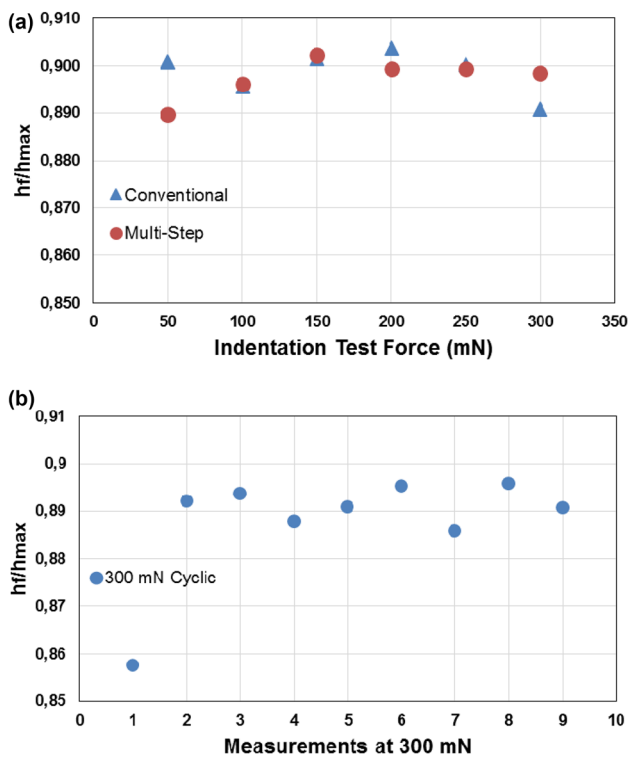


Fig. 9 **a** Pile-up effect for three different tests (conventional, multi-step) and **b** 300 mN cyclic on DP 800

the material is an important factor for pile-up and sink-in behavior. They noted that no pile-up occurs for the materials with $n > 0.3$, whereas for the materials with n value smaller 0.3, $h_f/h_{max} = 0.12$ is the turning point above which pile-up is encountered. As it can be inferred from the above studies, h_f/h_{max} ratio cannot be used as the sole criterion to report pile-up effect and the critical value may change from one material to another. Gale et al. [54] concluded that even the h_f/h_{max} ratio is beneficial in terms of determining pile-up or sink-in occurrence, it is not accurate for estimating the pile-up characteristics. Similarly, it was reported by Ekmekci et al. [55] that h_f/h_{max} values for sintered copper powder compacts, and copper sheet were obtained in the range of 0.90–0.97 yet no pile-up effect was observed due to work-hardening and subsequent sintering effect. Figure 9 shows the h_f/h_{max} values as a function of indentation force for both conventional, multi-step and 300 mN cyclic types of loading. Average values for h_f/h_{max} was calculated as 0.897. It is very well known fact that DP 800 exhibits work-hardening (as shown in Fig. 1) and pile-up is not at a significant level.

4 Conclusion

The effect of indentation loading type and level was investigated for an advanced high strength steel grade DP 800 material. Three different loading conditions, namely conventional, cyclic and multi-step was experimented in microindentation. The followings are the main outcomes of this research:

- In conventional indentation, six different indentation peak forces were experimented from 50 to 300 mN, and Young's modulus values were recorded in the range of 192–227 GPa, while hardness values were in the range of 3.17–3.62 GPa. Relatively less scattered hardness data resulted from the fact that the chosen indentation forces lead to overall material response rather than steel phases namely ferrite and martensite.
- Cyclic indentations were performed at 300 mN level and average hardness and Young's modulus values were obtained as 3.57 GPa, and 187.7 GPa, respectively. In multi-step indentation, on the other hand, the indentation force level was increased from 0 to 300 mN with 50 mN step size. It was observed that both Young's modulus and hardness values were decreased with the increasing indentation force which is called as an indentation size effect. The indentation size effect was found to be more pronounced with lower loads.
- To reveal the effect of different indentation peak forces on the hardness and Young's modulus data indentation were analyzed using one-way ANOVA ($p \leq 0.05$). It was revealed that changes in both Young's modulus and hardness values with peak indentation forces are insignificant for the force levels (50–300 mN) experimented.

Acknowledgements This work was partially supported by The Scientific and Technological Council of Turkey (TUBITAK) under Grant No. 218M913. The authors are also grateful to Prof. Dr. Uğur Kölemen and Assoc. Prof. Dr. Fikret Yılmaz of Gaziosmanpaşa University for sharing their lab capabilities and their assistance in microindentation tests. We extend our gratitude to SSAB for providing test materials used in this study.

References

1. P. Ferro, A. Tiziani, Metallurgical and mechanical characterization of electron beam welded DP600 steel joints. *J. Mater. Sci.* **47**, 199–207 (2012)
2. X. Hu, K.S. Choi, X. Sun, Y. Ren, Y. Wang, Determining individual phase flow properties in a quench and partitioning steel with in situ high-energy X-ray diffraction and multiphase elasto-plastic self-consistent method. *Metall. Mater. Trans. A* **47**, 5733–5749 (2016)

3. B. Johansson, K. Olsson, Tooling solutions for advanced high strength steel, in: Uddeholm Automotive Tooling Seminar, February 9–11, 2005, Sunne, Sweden
4. R. Kuziak, R. Kawalla, S. Waengler, Advanced high strength steels for automotive industry. *Arch. Civ. Mech. Eng.* **8**, 103–117 (2008)
5. Ö.N. Cora, Development of rapid die wear test method for assessment of dielife and performance in stamping of Advanced/Ultra High Strength Steel (A/UHSS) sheet materials, Ph.D Dissertation, Virginia Commonwealth University, Richmond, VA, USA, (2009)
6. E.V. Nesterova, S. Bouvier, B. Bacroix, Microstructure evolution and mechanical behavior of a high strength dual-phase steel under monotonic loading. *Mater. Charact.* **100**, 152–162 (2015)
7. S. Keeler, M. Kimchi, P.J. Mooney, Advanced high-strength steels—application Guidelines v.6.0, World Auto Steel, (2017)
8. N.H. Abid, R.K.A. Al-Rub, A.N. Palazotto, Micromechanical finite element analysis of the effects of martensite morphology on the overall mechanical behavior of dual phase steel. *Int. J. Solids Struct.* **104–105**, 8–24 (2017)
9. M.I. Khan, M.L. Kuntz, E. Biro, Y. Zhou, Microstructure and mechanical properties of resistance spot welded advanced high strength steels. *Mater. Trans.* **49**, 1629–1637 (2008)
10. K. Hayashi, K. Miyata, F. Katsuki, T. Ishimoto, T. Nakano, Individual mechanical properties of ferrite and martensite in Fe-0.16 mass% C–1.0 mass% Si-1.5 mass% Mn steel. *J. Alloy. Compd.* **577**, S593–S596 (2013)
11. F. Zhang, A. Ruimi, D.P. Field, Phase identification of dual-phase (DP980) steels by electron backscatter diffraction and nanoindentation techniques. *Microsc. Microanal.* **22**, 99–107 (2016)
12. V.H. Baltazar-Hernandez, S.K. Panda, M.L. Kuntz, Y. Zhou, Nanoindentation and microstructure analysis of resistance spot welded dual phase steel. *Mater. Lett.* **64**, 207–210 (2010)
13. G. Cheng, F. Zhang, A. Ruimi, D.P. Field, X. Sun, Quantifying the effects of tempering on individual phase properties of DP980 steel with nanoindentation. *Mat. Sci. Eng. A* **667**, 240–249 (2016)
14. A.E. Giannakopoulos, S. Suresh, Determination of elastoplastic properties by instrumented sharp indentation. *Scr. Mater.* **40**, 1191–1198 (1999)
15. L. Qian, M. Li, Z. Zhou, H. Yang, X. Shi, Comparison of nano-indentation hardness to microhardness. *Surf. Coat. Tech.* **195**, 264–271 (2005)
16. M.Y. N'Jock, F. Roudet, M. Idriss, O. Bartier, D. Chicot, Work-of-indentation coupled to contact stiffness for calculating elastic modulus by instrumented indentation. *Mech. Mater.* **94**, 170–179 (2016)
17. C.D. Hardie, S.G. Roberts, A.J. Bushby, Understanding the effects of ion irradiation using nanoindentation techniques. *J. Nucl. Mater.* **462**, 391–401 (2015)
18. I. Sapezanskaia, J.J. Roa, G. Fargas, M. Turon-Viñas, T. Trifonov, R. Kouitat-Njiwa, A. Redjaimia, A. Mateo, Deformation mechanisms induced by nanoindentation tests on a metastable austenitic stainless steel: a FIB/SIM investigation. *Mater. Charact.* **131**, 253–260 (2017)
19. L. Zhu, B. Xu, H. Wang, C. Wang, D. Yang, Measurement of mechanical properties of 1045 steel with significant pile-up by sharp indentation. *J. Mater. Sci.* **46**, 1083–1086 (2011)
20. K.H. Chung, W. Lee, J.H. Kim, C. Kim, S.H. Park, D. Kwon, K. Chung, Characterization of mechanical properties by indentation tests and FE analysis—validation by application to a weld zone of DP590 steel. *Int. J. Solids Struct.* **46**, 344–363 (2009)
21. Z.H. Xu, D. Rowcliffe, Method to determine the plastic properties of bulk materials by nanoindentation. *Philos. Mag.* **82**, 1893–1901 (2002)
22. F. Ye, X. Sun, Nanoindentation response analysis of TiN–Cu coating deposited by magnetron sputtering. *Progress Nat. Sci. Mater. Inter.* **28**, 40–44 (2018)
23. M. Szala, M. Walczak, K. Pasierbiewicz, M. Kaminski, Cavitation erosion and sliding wear mechanisms of AlTiN and TiAlN films deposited on stainless steel substrate. *Coatings* **9**, 340 (2019)
24. B. Bor, D. Giuntini, B. Domènech, M.V. Swain, G.A. Schneider, Nanoindentation-based study of the mechanical behavior of bulk supercrystalline ceramic-organic nanocomposites. *J. Eur. Ceram. Soc.* **39**, 3247–3256 (2019)
25. A. Tiwari, S. Natarajan, *Applied Nanoindentation in Advanced Materials* (Wiley, New York, 2017)
26. F. Zhang, A. Ruimi, P.C. Wo, D.P. Field, Morphology and distribution of martensite in dual phase (DP980) steel and its relation to the multiscale mechanical behavior. *Mat. Sci. Eng. A* **659**, 93–103 (2016)
27. I. Diego-Calderón, M.J. Santofimia, J.M. Molina-Aldareguia, M.A. Monclús, I. Sabirov, Deformation behavior of a high strength multiphase steel at macro- and micro-scales. *Mat. Sci. Eng. A* **611**, 201–211 (2014)
28. H. Ghassemi-Armaki, R. Maaß, S.P. Bhat, S. Sriram, J.R. Greer, K.S. Kumar, Deformation response of ferrite and martensite in a dual-phase steel. *Acta Mater.* **62**, 197–211 (2014)
29. M.D. Taylor, K.S. Choi, X. Sun, D.K. Matlock, C.E. Packard, L. Xu, F. Barlat, Correlations between nanoindentation hardness and macroscopic mechanical properties in DP980 steels. *Mat. Sci. Eng. A* **597**, 431–439 (2014)
30. R. Rodriguez, I. Gutierrez, Correlation between nanoindentation and tensile properties: influence of the indentation size effect. *Mat. Sci. Eng. A* **361**, 377–384 (2003)
31. Docol DP/DL Cold reduced dual phase steels, Datasheet: 13-02-14 GB8201 DOCOL, SSAB (2014)
32. W. Wang, X. Wei, The effect of martensite volume and distribution on shear fracture propagation of 600–1000 MPa dual phase sheet steels in the process of deep drawing. *Int. J. Mech. Sci.* **67**, 100–107 (2013)
33. X. Chen, I.A. Ashcroft, R.D. Wildman, C.J. Tuck, A combined inverse finite element - elastoplastic modelling method to simulate the size-effect in nanoindentation and characterise materials from the nano to micro-scale. *Int. J. Solids Struct.* **104–105**, 25–34 (2017)
34. D.J. Shuman, A.L.M. Costa, M.S. Andrade, Calculating the elastic modulus from nanoindentation and microindentation reload curves. *Mater. Charact.* **58**, 380–389 (2007)
35. H.R. Lashgari, J.M. Cadogan, D. Chu, S. Li, The effect of heat treatment and cyclic loading on nanoindentation behaviour of FeSiB amorphous alloy. *Mater. Design.* **92**, 919–931 (2016)
36. T. Saraswati, T. Sritharan, S. Mhaisalkar, C.D. Breach, F. Wulff, Cyclic loading as an extended nanoindentation technique. *Mater. Sci. Eng. A* **423**, 14–18 (2006)
37. A. Chabok, E. Galinmoghaddam, J.T.M. De Hosson, Y.T. Pei, Micromechanical evaluation of DP1000-GI dual-phase high-strength steel resistance spot weld. *J. Mater. Sci.* **54**, 1703–1715 (2019)
38. J.J. Roa, I. Sapezanskaia, G. Fargas, R. Kouitat, A. Redjaimia, A. Mateo, Dynamic deformation of metastable austenitic stainless steels at the nanometric length scale. *Metall. Mater. Trans. A* **49**, 6034–6039 (2018)
39. J. Wu, Y. Pan, J. Pi, Nanoindentation study of Cu₅₂Zr₃₇Ti₈In₃ bulk metallic glass. *Appl. Phys. A* **115**(1), 305–312 (2014)
40. C.J. Chen, K. Yan, L. Qin, M. Zhang, X. Wang, T. Zou, Z. Hu, Effect of heat treatment on microstructure and mechanical properties of laser additively manufactured AISI H13 tool steel. *J. Mater. Eng. Perform.* **26**, 5577–5589 (2017)
41. R.A. Rijkenberg, M.P. Aarnts, F.A. Twisk, M.J. Zuijderwijk, M. Knieps, H. Pfaff, Linking crystallographic, chemical and

- nano-mechanical properties of phase constituents in DP and TRIP steels. *Mater. Sci. Forum* **638–642**, 3465–3472 (2010)
42. C.A. Schuh, Nanoindentation studies of materials. *Mater. Today* **9**, 32–40 (2006)
 43. M. Ruiz-Andres, A. Conde, J. Damborenea, I. Garcia, Microstructural and micromechanical effects of cold roll-forming on high strength dual phase steels. *Mater. Res.* **18**, 843–852 (2015)
 44. M. Delincé, P.J. Jacques, T. Pardoën, Separation of size-dependent strengthening contributions in fine-grained dual phase steels by nanoindentation. *Acta Mater.* **54**, 3395–3404 (2006)
 45. D. Pan, T.G. Nieh, M.W. Chen, Strengthening and softening of nanocrystalline nickel during multistep nanoindentation. *Appl. Phys. Lett.* **88**, 161922 (2006)
 46. P. Cavaliere, Mechanical properties of nanocrystalline materials, in *Handbook of mechanical nanostructuring*, ed. by M. Aliofk-hazraei (Wiley-VCH, Singapore, 2015), p. 8
 47. C. Feng, B.S. Kang, Young's modulus measurement using a simplified transparent indenter measurement technique. *Exp. Mech.* **48**, 9–15 (2008)
 48. A. Richter, C.P. Daghljan, R. Ries, V.L. Solozhenko, Investigation of novel superhard materials by multi-cycling nanoindentation. *Diam. Relat. Mater.* **15**, 2019–2023 (2006)
 49. J. Wei, B.L. McFarlin, A.J.W. Johnson, A multi-indent approach to detect the surface of soft materials during nanoindentation. *J. Mater. Res.* **31**, 2672–2685 (2016)
 50. Z.S. Ma, Y.C. Zhou, S.G. Long, C. Lu, On the intrinsic hardness of a metallic film/substrate system: indentation size and substrate effects. *Int. J. Plast.* **34**, 1–11 (2012)
 51. J. Nohava, R. Mušálek, J. Matějčíček, M. Vilémová, A contribution to understanding the results of instrumented indentation on thermal spray coatings—case study on Al₂O₃ and stainless steel. *Surf. Coat. Tech.* **240**, 243–249 (2016)
 52. Y. Mazaheri, A. Kermanpur, A. Najafzadeh, Nanoindentation study of ferrite–martensite dual phase steels developed by a new thermomechanical processing. *Mat. Sci. Eng. A* **639**, 8–14 (2015)
 53. A. Bolshakov, G.M. Pharr, Influences of pileup on the measurement of mechanical properties by load and depth sensing indentation techniques. *J. Mater. Res.* **13**, 1049–1058 (1998)
 54. J.D. Gale, A. Achuthan, The effect of work-hardening and pile-up on nanoindentation measurements. *J. Mater. Sci.* **49**, 5066–5075 (2014)
 55. D. Ekmekci, F. Yılmaz, U. Kölemen, Ö.N. Cora, Microindentation on the porous copper surface modulations. *Appl. Phys. A* **123**, 705 (2017)

Publisher's Note Springer Nature remains neutral with regard to jurisdictional claims in published maps and institutional affiliations.